ONE HUNDRED NEURAL NETWORKS AND BRAINS WATCHING VIDEOS: LESSONS FROM ALIGNMENT

Anonymous authors
Paper under double-blind review

ABSTRACT

What can we learn from comparing video models to human brains, arguably the most efficient and effective video processing systems in existence? Our work takes a step towards answering this question by performing the first large-scale benchmarking of deep video models on representational alignment to the human brain, using publicly available models and a recently released video brain imaging (fMRI) dataset. We disentangle four factors of variation in the models (temporal modeling, classification task, architecture, and training dataset) that affect alignment to the brain, which we measure by conducting Representational Similarity Analysis across multiple brain regions and model layers. We show that temporal modeling is key for alignment to brain regions involved in early visual processing, while a relevant classification task is key for alignment to higher-level regions. Moreover, we identify clear differences between the brain scoring patterns across layers of CNNs and Transformers, and reveal how training dataset biases transfer to alignment with functionally selective brain areas. Additionally, we uncover a negative correlation of computational complexity to brain alignment. Measuring a total of 99 neural networks and 10 human brains watching videos, we aim to forge a path that widens our understanding of temporal and semantic video representations in brains and machines, ideally leading towards more efficient video models and more mechanistic explanations of processing in the human brain.

1 INTRODUCTION

Humans are extremely efficient in processing the constant streams of visual information they receive, relying on motion and temporal information on top of visual semantics to understand their environment (Sekuler et al., 2002). How current state-of-the-art video models compare to that standard is a question that is often addressed by comparing their performance to human baselines (Zhou et al., 2018a; Andonian et al., 2020), but is much more under-explored with respect to internal representations. Representational alignment was recently defined in Sucholutsky et al. (2023) as "the extent to which the internal representations of two or more information processing systems agree". It is a cornerstone of cognitive computational neuroscience (Kriegeskorte & Douglas, 2018), a discipline that aims to identify neural mechanisms underlying cognition by employing task-performing computational models, such as deep neural networks, for hypothesis testing. This has been shown to be a highly progressive research program yielding novel neuroscientific insights (Doerig et al., 2023). Identifying model design choices that strongly impact alignment can not only shed light on the underlying brain mechanisms, but also guide machine learning on borrowing brain's advantages such as efficiency and robustness, for example using brain-aligned designs as starting points for further model development Lu et al. (2024b). Our work aims to fill the gap in exploring the representational alignment of deep video models to the human brain, joining and increasing understanding of temporal modeling in brains and machines, and pointing towards more efficient video models.

Human visual information processing has classically been separated into two separate streams, ventral and dorsal (Mishkin et al., 1983). The ventral stream is thought to process more static information and the dorsal stream more dynamic information (Kravitz et al., 2011), whereby a motion area MT (Culham et al., 2001) has also been identified. More recent work found evidence for a third visual pathway specializing in dynamic social perception (Pitcher & Ungerleider, 2021; Küçük et al., 2024). Another organizing principle that has been identified in human visual processing is a hierarchy of temporal receptive fields, with temporal integration extending over longer time-scales in higher compared to lower visual areas (Hasson et al., 2008; Zhou et al., 2018b; Groen et al., 2022;

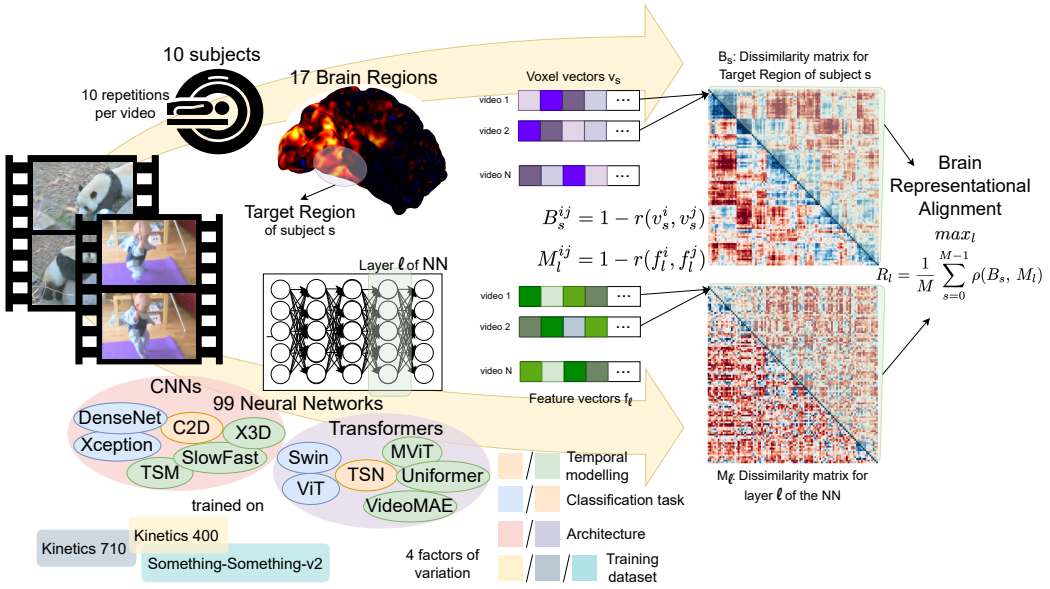

Figure 1: Overview of our pipeline for benchmarking video models on brain representational alignment. We systematically compare 99 neural networks across 4 factors of variation on their alignment with fine-grained brain regions measured with Representational Similarity Analysis.

Brands et al., 2024). These neuroscience findings collectively suggest the presence of specialized mechanisms for motion and temporal information processing in the human brain.

In video AI, specifically machine learning, temporal information is usually modeled as a third input dimension, using mechanisms such as 3D convolutions (Tran et al., 2015; Carreira & Zisserman, 2017); however there are only limited similarities with processing in the brain, as the effective temporal receptive fields in these networks usually stay constant throughout processing layers. Older models handling RGB images and optical flow as separate streams (Simonyan & Zisserman, 2014) bear some resemblance to dual-stream processing in the brain, but most successful designs fall far from direct comparison (Feichtenhofer et al., 2019; Lin et al., 2019). Recent papers focus on video Transformers (Liu et al., 2022; Wang et al., 2023b), including hybrids to combine benefits of CNNs and Transformers (local structure and long term dependencies) in temporal modeling (Li et al., 2022; 2023a). Comparing the variety in engineering solutions from video-AI to the way humans process video can help adjudicate between models in terms of their ability to capture the temporal aspects of information processing in the brain and increase understanding on the representations they compute.

A line of work has recently set path in large-scale systematic benchmarking of models on representational alignment, to both the human brain and behavior (Conwell et al., 2022; Muttenthaler et al., 2023), advancing the understanding of how these models internally compare to humans on a common basis. However, these works have so far been limited to the domain of static images; a comprehensive analysis of video model alignment with human video processing is still lacking.

Our contributions:

- We perform the first large scale benchmarking of video models on human brain representational alignment, on a recent publicly released video fMRI dataset. Specifically, we consider 47 video models for action recognition and 41+11 image models for object and action recognition.
- We decouple the alignment effects of temporal modeling from those of action space optimization by adding image action recognition models as control, as well as examine the impact of model architecture and training dataset, all comparing across a fine-grained variety of brain regions.
- We show that temporal modeling is the important factor for representational alignment to early brain regions, while action space optimization for alignment to late brain regions. We find distinct patterns emerging in different processing stages of CNNs and Transformers, along with an effect of training biases on alignment to functionally selective areas.
- We report a significant negative correlation of model FLOPs to alignment in several high-level brain areas, indicating that computationally efficient neural networks can potentially produce more human-like semantic representations.

2 Related Work

Large scale brain datasets. Compared to artificial intelligence, the field of computational cognitive neuroscience has been exposed to the concept of benchmarking only recently (Schrimpf et al., 2020), with the majority of prior works consisting of stand-alone assessments of model-human representational alignment on their own brain data for one or a few models. Works such as BrainScore (Schrimpf et al., 2018) and the Algonauts challenges (Cichy et al., 2019; 2021; Gifford et al., 2023) have set the stage for representational alignment research on benchmark datasets where any model can be compared and comparisons can be widely accessed by everyone in the community, generating new insights via data-driven exploration and field-mapping. Datasets such as NSD (Allen et al., 2022) and THINGS (Hebart et al., 2023) have been established as benchmark image stimuli brain imaging datasets due to their size and high signal quality. For video stimuli, there has also been some recent development (Dima et al., 2022; Zhou et al., 2023; McMahon et al., 2023) that is mostly focused on social actions. Most recently the Bold Moments Dataset (BMD) (Lahner et al., 2024) was introduced, putting forth a large-scale, highly reliable dataset with extensive quality control to ensure suitability for AI model comparisons. *In this work,* we conduct the first extensive benchmarking of a total of 99 models on representational alignment with the fMRI data in BMD.

Measures of model-brain alignment. The two most widely used approaches for measuring brain-model alignment are voxel-wise encoding (Güçlü & Van Gerven, 2015) and Representational Similarity Analysis (RSA) (Kriegeskorte et al., 2008). The former involves training a linear regression to predict voxel space from a model's feature space and conduct all analyses there, and inherently models each voxel response independently, rather than how voxels respond together. The latter projects both spaces into a third common space of pairwise condition patterns; it works by computing a distance metric between the representations of each pair of test conditions for both voxel and feature space, forming the Representational Dissimilarity Matrix (RDM), which reflects differences between patterns of activity within populations of voxels. There are several influential works assessing model-brain alignment for static images, using both voxel-wise encoding (Eickenberg et al., 2017; St-Yves & Naselaris, 2018; La Tour et al., 2022) and RSA (Cichy et al., 2016; Dobs et al., 2019; King et al., 2019; Bartnik et al., 2024) as well as methods combining the two approaches (Dwivedi et al., 2021; Konkle & Alvarez, 2022; Conwell et al., 2022). Many of these works validate the image models' alignment to the brain's early-to-late processing hierarchy, as has also been shown with speech models (Millet et al., 2022), but it has not been seen if a similar mapping can be found in video models. *In this work,* we use RSA to derive the representational alignment between the features of each neural network's layers and the voxels in each brain Region of Interest (ROI) in BMD, contrasting this alignment between early and late stages of visual processing.

Model-brain alignment benchmarking. Extensive benchmarking in the image domain was conducted by Conwell et al. (2022) on NSD, who decoupled multiple factors that give rise to differences between image models, specifically model architecture, diet (training dataset), and training task, which they varied one at a time keeping all others constant, to assess which factors most influence model-brain alignment. A similar approach was followed in Wang et al. (2023a) to examine the effect of contrastive learning on model-brain alignment. There are also several works extensively benchmarking neural networks on alignment to human behavior, through behavioral similarity judgment data, e.g. Muttenthaler et al. (2023) and Marjieh et al. (2023), where the latter also includes three video action recognition models. In Mineault et al. (2021) a limited testing of five video action recognition models was performed, to compare against their own model trained with a custom objective. More recently, a study by Garcia et al. (2024) focused on social-action videos and conducted a first, yet limited, video benchmarking by testing eight video models against 200 image models. *In this work,* we include 47 video models for action class recognition and 41+11 image models for object and action class recognition. Inspired by Conwell et al. (2022), we are interested in disentangling the role of different factors, and thus we vary the models' architecture by contrasting CNNs to Transformers, and the models' training dataset by contrasting three different datasets. Importantly, we control for the change in task when comparing object recognition image models to action recognition video models, through varying one factor at a time by further comparing with image models trained for action class recognition. In addition to Conwell et al. (2022), our work provides a more fine-grained analysis that addresses specific brain regions instead of the visual cortex as a whole. In contrast to Garcia et al. (2024), we compare an equally large number of video models to image models, on top of the important control of the training task and the comparison between different architectures and training dataset, and use RSA instead of voxel-wise encoding.

3 METHODOLOGY

In Figure 1 we show an overview of our methodology for measuring alignment of video models to the human brain. In the next three sections, we describe the design choices of the alignment measure, the video models, and the brain imaging dataset.

3.1 ALIGNMENT BY REPRESENTATIONAL SIMILARITY ANALYSIS

We start by motivating our choice of metric to measure the alignment between a neural network and a brain region. To observe patterns of activity that consider the interactions between groups of voxels (multivariate analysis), either Representational Similarity Analysis (RSA) (Kriegeskorte et al., 2008) or a combined approach that performs RSA on top of voxel-wise encoding (mixedRSA or veRSA Khaligh-Razavi et al. (2017)) are good candidates. Conwell et al. (2022) extensively compared these methods and showed that veRSA often fails to uncover differences between models in terms of brain alignment. This is likely due to the fact that voxel-wise encoding allows for re-weighting of the model activations while mapping them to the brain, thereby optimizing brain predictivity but obscuring how the model representations correlate with brain responses out of the box. Based on our intent to benchmark the emergent alignment of AI models, we choose RSA as a stricter metric that can uncover more potential differences between models.

Representational Dissimilarity Matrix (RDM) computation. For a brain Region of Interest (ROI) of a human subject s with voxel vectors v_s and a model layer l with feature vectors f_l, the brain RDM (B_s) and model RDM (M_l) are calculated as follows:

$$B_s^{ij} = 1 - r(v_s^i, v_s^j), \quad M_l^{ij} = 1 - r(f_l^i, f_l^j), \quad \forall i, j (i < j), \;\; 0 \leq j < N, \tag{1}$$

where N is the total number of videos and r is the Pearson correlation, resulting in RDMs that are symmetric with size $N(N-1)/2$. To obtain v_s we first average the voxels across measurements from all K repetitions of a stimulus video i, so $v_s^i = \frac{1}{K}\sum_{k=0}^{K-1} v_{s,k}^i$. To create f_l we first reduce the dimensionality of the original features to 100 Principal Components using Principal Component Analysis (PCA). We provide a comparison with Sparse Random Projection (SRP) and the full dimensions in Appendix D. No standardization is performed on the voxel and feature vectors, neither across videos nor across features to avoid distortions (Walther et al., 2016).

Correlation of RDMs. To derive the alignment of a model layer and a brain ROI, we correlate each layer RDM of each model (M_l) with each subject RDM of each ROI (B_s) using Spearman correlation (ρ), and then average the correlations across subjects for each model layer:

$$R_l = \frac{1}{M}\sum_{s=0}^{M-1} \rho(B_s,\, M_l), \tag{2}$$

where M is the total number of subjects. In analyses where we show only one correlation value for the alignment of a whole model and a brain ROI, this is computed by $R = max_l(R_l)$, i.e., the highest-correlating layer in the model.

Noise ceiling computation. Because of individual subject variability in brain data, noise ceilings for each ROI are computed to compare model RSA scores against the maximum obtainable score given the inter-subject variability (Nili et al., 2014). For the lower noise ceiling (LNC) we compute a mean RDM across all subjects except one. Then we take the Spearman correlation of the left-out subject RDM and mean RDM. We do this for all the subjects and then calculate the average correlation:

$$LNC = \frac{1}{M}\sum_{j=0}^{M-1}(\rho(\frac{1}{M}\sum_{i=0, i\neq j}^{M-1} B_i,\;\; B_j)). \tag{3}$$

For the upper noise ceiling (UNC) we take the mean of all RDMs without removing subjects and compute the Spearman correlation of each subject RDM with the mean RDM, and average:

$$UNC = \frac{1}{M}\sum_{j=0}^{M-1}(\rho(\frac{1}{M}\sum_{i=0}^{M-1} B_i,\;\; B_j)). \tag{4}$$

The upper noise ceiling signifies perfect correlation for the amount of noise in this ROI's data, often referred to as the maximum amount of variance that can be explained.

Table 1: Model families benchmarked. We sample the same number of CNN and Transformer image object recognition models as in our maximal set of video models. We also test 10 image models trained on action recognition; this division is shown with the grouping on the right. Action recognition models are on Kinetics 400; those also available on other datasets are marked by a,b.

Image Object Recognition				**Action Recognition**				
	CNNs		**Transformers**		**CNNs**		**Transformers**	
1	AlexNet	2	CAiT	6	CSN	2	MViTv2[b]	**Video**
2	DenseNet	2	ConViT	5	I3D	2	TimeSformer	
2	EfficientNet	2	DEiT	1	R2P1D	2	Uniformer	
2	RegNet	2	MViTv2	2	SlowFast	2	Uniformerv2[a]	
4	ResNet	3	Swin	4	Slow[a]	1	VideoMAE	
2	ResNeXt	1	Twins	1	TaNet	2	VideoMAEv2	
4	VGG	2	ViT	1	TPN	3	VideoSwin[a]	
2	WideResNet			5	TSM[b]			
2	Inception			2	X3D			
2	RepVGG							**Image**
2	SeResNe(X)t			4	C2D	1	TimeSformer	
2	Xception			4	TSN[b]	1	TSN	
27		14		27+8		14+2		

[a] Availability also on Kinetics 710 (Carreira et al., 2019)
[b] Availability also on Something-Something-v2 (Goyal et al., 2017)

Statistical significance. To test if model RDMs correlated significantly with brain RDMs, we performed permutation tests (Nili et al., 2014). For each model we permute the rows of all layer RDMs $1,000$ times using the same $1,000$ random permutations for all models and layers. We then calculate a null distribution by computing the Spearman correlations of all permuted RDMs with each subject RDM, and average the resulting null distributions across subjects separately for each model layer. For significance of a group of models against zero, we perform a two-tailed sign test between the median null distribution of all models in the group and the median observed Spearman correlation. To test for significant differences between two groups of models, we perform a two-tailed sign test between the null distribution created from the across-group differences in the within-group median distributions, and the observed difference in the medians of the two model groups' Spearman correlations. We correct for multiple comparisons between model groups by applying Bonferroni correction equal to the number of group pairwise combinations.

3.2 Video Models

Our goal was to benchmark as many publicly released video models as possible, sampling from different architectures (e.g. CNNs, Transformers) as equally as possible, while differentiating the effects of optimizing for the action classification task and temporal modeling on brain alignment.

Model choice. In total, we benchmark 99 models; of these, 41 are image models trained for object recognition on ImageNet, 10 are image models trained for action recognition on Kinetics 400 (Kay et al., 2017), and 41 are video models trained for action recognition on Kinetics 400. The distinction between the last two is made based on whether the models treat time in a non-trivial way, where trivial is considered anything that makes completely separate computations per frame and only averages frame features before classification, or aggregates frames with static pooling operations at different stages. The remaining 7 models are trained for action recognition on other datasets, namely Kinetics 710 (Carreira et al., 2019) and Something-Something-v2 (Goyal et al., 2017). Image models trained on object recognition were ported from torchvision[1] and timm[2], while image and video models trained on action recognition were ported from mmaction2[3]. The main families of models used are listed in Table 1, while a full list of all the model versions used can be found in Appendix B.

Model feature extraction. We perform preprocessing according to the functions provided by the models' sources (torchvision, timm, or mmaction2). Regarding the temporal dimension, for image models trained on ImageNet we perform inference for all frames and then average the features, while action recognition image models were trained on sequences of frames as input samples (only

[1] https://pytorch.org/vision/main/models.html
[2] https://huggingface.co/models?library=timm
[3] https://mmaction2.readthedocs.io/en/latest/model_zoo/recognition.html

to aggregate with trivial pooling operations), so for those we perform inference on video inputs, as we do for video models. Because each model expects a specific length of timepoints sampled at a specific rate, different size batches of sub-clips are created per video and model, and the resulting sub-clip features are averaged for the whole video. We extract features from all higher-level blocks in the models (e.g., in a ResNet-type model of five blocks with four layers each, we extract features at the end of each block) and also include the final fully connected classification layer. We flatten the features after extraction, producing a single one-dimensional feature vector per layer.

3.3 Brain Dataset

We utilize the Bold Moments Dataset (BMD) (Lahner et al., 2024) consisting of whole-brain 3T fMRI recordings ($2.5 \times 2.5 \times 2.5$ mm voxels, resampled TR of 1s) from 10 subjects watching $1,102$ 3s videos from the Moments in Time (Monfort et al., 2019) and Multi-Moments in Time (Monfort et al., 2021) video datasets. Extensive details on the fMRI data acquisition can be found in (Lahner et al., 2024); a summary is provided in Appendix A. For each subject, $1,000$ videos were shown for 3 repetitions and those recordings make up the "training set", whereas 102 videos were shown for 10 repetitions and make up the "test set". In our analysis, we only use the 102 videos of the test set, whose high number of repetitions allows for the application of RSA. We report partial results on the 1000 video training set in Appendix D showing noise increase from insufficient repetitions. The test set videos are sensibly representative of the videos present in the whole dataset. Specifically, roughly 25% of the videos are close-ups of small children, 22% are close-ups of animals, another 22% are humans doing sports, 10% are scenes with motion without visible humans or animals (e.g. a waterfall, a car), 6% people cooking, and 6% people performing some other form of manual labour.

Preprocessing and Regions of Interest (ROIs). We used preprocessed data provided by (Lahner et al., 2024). A summary of the most important preprocessing steps, including anatomical alignment and ROI definitions, is again provided in Appendix A. From the available brain ROIs, we first joined the two hemispheres by concatenating the voxels corresponding to each pair of areas, and then also joined the dorsal and ventral parts of V1 and V2. We group ROIs based on their anatomical location on the brain (Grill-Spector & Malach, 2004), in four groups: Early Visual Cortex (includes areas V1, V2, V3v, V3d), Ventral-Occipital Stream (hV4, OFA, LOC, FFA, PPA), Dorsal Stream (V3ab, IPS0, IPS1-3, RSC), and Lateral Stream (EBA, TOS, MT, STS). Areas in Early Visual Cortex are considered early areas of processing, hV4 and V3ab are considered intermediate, and the rest are considered late areas of visual processing, based on the flow of information through the brain.

4 Results

Differences in brain alignment between 99 neural networks processing videos could be related to a number of factors. In the following sections we systematically examine the following factors: temporal modeling, classification task, architecture design, and training dataset. Finally, we also investigate how brain alignment relates to the models' computational complexity.

Video vs. Image models, controlling for the classification task. First, we compare models by varying the temporal modeling (Video vs. Image) and controlling for the classification task (object vs. action recognition) while keeping the training dataset constant (action recognition on Kinetics 400). In Figure 2a we observe that in the Early Visual Cortex, video models score significantly higher than the image models, while image models trained on action recognition may even capture less variance than the image models trained on object recognition. The control for image models trained on action recognition decouples the effect of classification objective from temporal modeling, and shows that the latter is the determining factor out of the two for RSA scoring in the early visual cortex. In later areas it can be seen that here the classification objective exerts more influence on the RSA score, as the video models do not fare much better than image models trained on action recognition, and those in general score higher than image models trained on object recognition. Out of all the later area groups, the Lateral stream shows the least significant differences. In relation to the noise ceilings, we observe that models are able to explain the largest amount of the total explainable variance in the Early Visual Cortex out of all brain regions (see Appendix D for a re-scaled plot by the UNC). In Figure 2b we notice that all three model categories exhibit an early-to-late hierarchy, with more shallow layers correlating the highest with early brain regions, and deeper layers correlating the highest with late brain regions. The mid-network representations

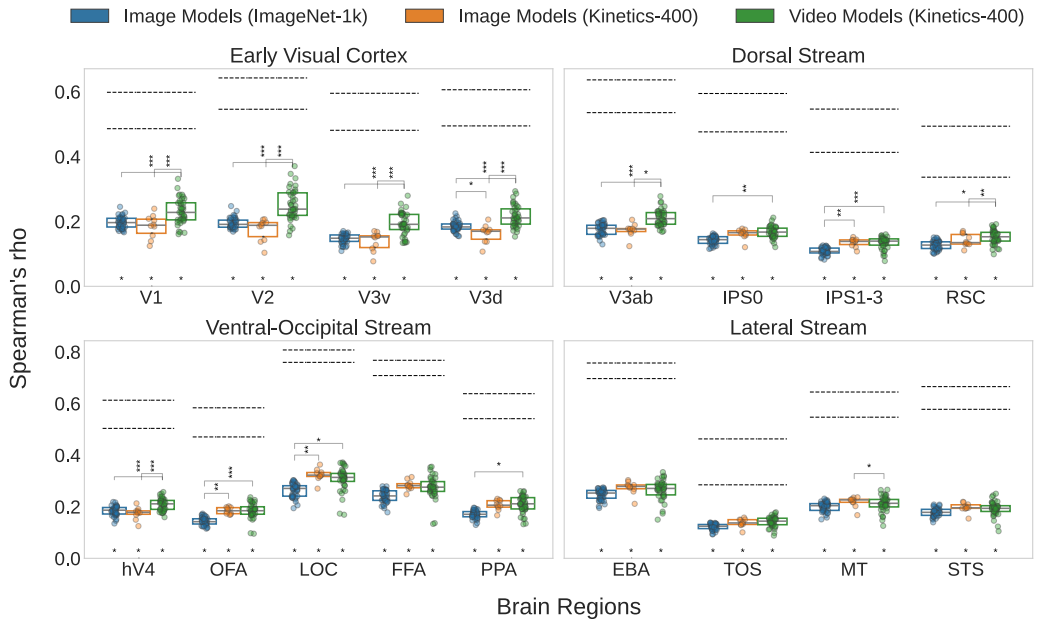

(a)

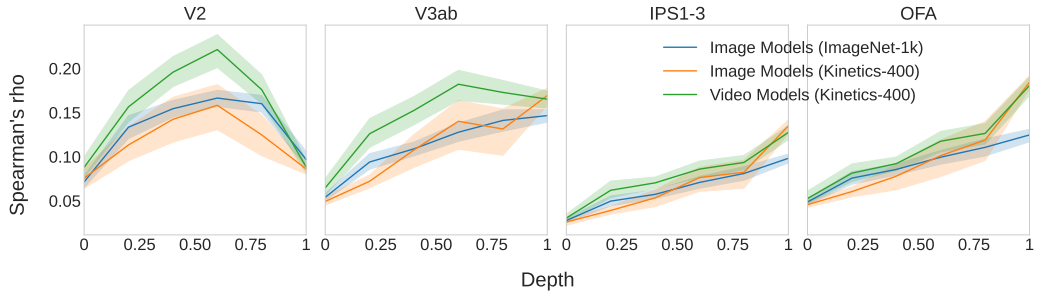

(b)

Figure 2: **Video vs. Image models, controlling for the classification task:** We find that temporal modeling is the important factor for representational alignment to early brain regions, while action space optimization for alignment to late brain regions, evaluating RSA score for a total of 92 models. In 2a we choose the best scoring layer for each model and show all 17 brain regions. Stars at $y = 0$ and on top of brackets indicate statistical significance against zero and significance of pairwise differences ($* : p < 0.05$, $** : p < 0.01$, $*** : p < 0.001$). Horizontal dashed lines show the upper and lower noise ceilings for each region. In 2b we show different model layer depths for regions chosen by zooming in on significant differences from 2a and sampling region groups evenly, the rest reported in Appendix C.

learned by the video models correlate better with V2 than those of image models, regardless if the latter are trained for action recognition. On the other hand for OFA, it is the representations in the classification layer of action recognition models that manage to match the brain better, even if there is no temporal modeling involved. In Figure 3 we point out that the top models are MViT, CSN, and SlowFast in V2, and CSN, TimeSformer, and VideoSwin in LOC. In V2 and for a portion of the subjects, the model MViT_v2_S comes close to capturing almost all of the explainable variance.

Varying the architecture. Next, we compare models by varying the architecture design (CNNs vs, Transformers), keeping temporal modeling, classification task, and training dataset all constant (video action recognition models trained on Kinetics 400). In Figure 4 we see that, in terms of the maximum score, Transformers and CNNs appear to be mostly equivalent, either of the two architectures taking the lead in different ROIs. Nevertheless, an interesting pattern appears when we analyse the changes in correlation across the models' layers. In V2 Transformers compute high correlating representations at a very shallow depth in the network (around 0.1 of the total depth), while CNNs much later, at around 0.6 of the total depth. In EBA, CNNs show a much clearer

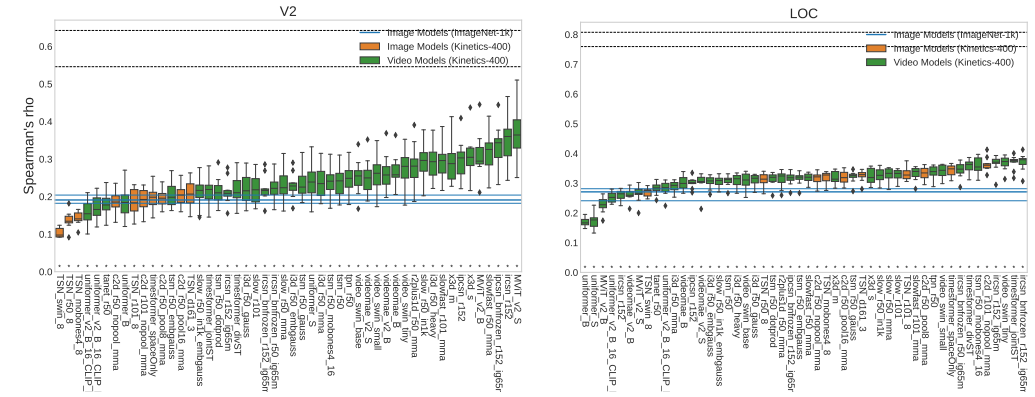

Figure 3: Ranking of all the Kinetics-400 action recognition models in RSA scoring order, against the baseline of image object recognition models. Top models in V2 are MViT, CSN, and SlowFast, while in LOC they are CSN, TimeSformer, and VideoSwin. Error bars signify variation across subjects. One early and one late region are shown (the two highest overall), the rest in Appendix C.

hierarchy, as correlation gradually increases with model depth, while Transformers have relatively stable representations up until the classification layer, where the score increases more abruptly. Still in EBA, Transformers explain more variance than CNNs when comparing only very shallow layers.

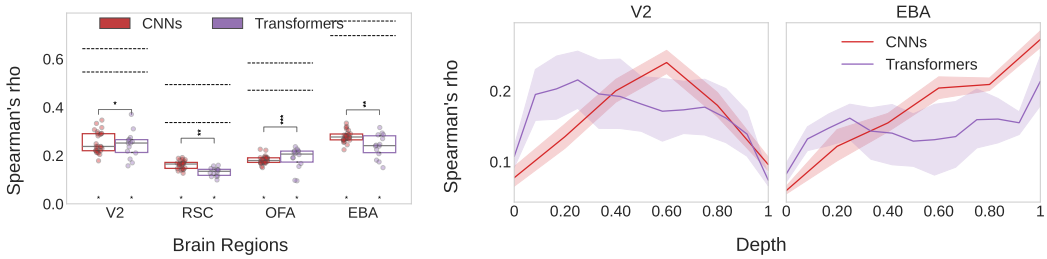

Figure 4: **Varying the architecture:** CNNs and Transformers are overall equivalent but exhibit striking differences in their score distribution across layer depths. We show RSA scores of 27 CNNs and 14 Transformers, for the best scoring model layer (4a) and all layer depths (4b). Brain regions showed are those exhibiting the most significant differences, sampling evenly from brain region groups. Exhaustive results can be found in Appendix C.

Varying the training dataset. Here, we compare models by varying the training dataset (Kinetics 400 vs. Kinetics 710 and Kinetics 400 vs. Something-Something-v2) and keeping all other factors constant through only including the exact same models trained on the two different datasets in each pair of dataset comparisons. In figure 5a we first observe that using models trained on an extended and enhanced version of the same dataset such as Kinetics 710 in relation to Kinetics 400, largely has no effect on brain alignment. However, when testing models trained on a more different domain, such as Something-Something-v2, some interesting differences emerge. In particular, there is a significant advantage of Kinetics 400 against Something-Something-v2 in FFA and OFA, and a somewhat similar pattern in LOC. In fact, this seems to show up both in shallow and deep layers of the models (figure 5b). Considering that Something-Something-v2 is a dataset that never shows faces and that FFA is the functionally selective region for faces, this result identifies that a dataset bias from the models' training can indeed be transferred to model-brain alignment for an ROI that is functionally selective specifically for this bias.

Relation to computational complexity. Last, we investigate how the brain correlation of action recognition models relates to their computational complexity (in FLOPs). In figure 6, we report a moderate but consistent negative correlation of model FLOPs to model-brain alignment especially in late ROIs of the Lateral and Dorsal Streams, with significant negative correlations observed in six ROIs, the top four of which are shown in 6b. In 6a we observe that although the significance of the negative relation is not present in all ROIs, the relation itself is consistent throughout the brain regions. A similar investigation for model parameters and model accuracy was performed but no consistent significant correlations were found (see Appendix E).

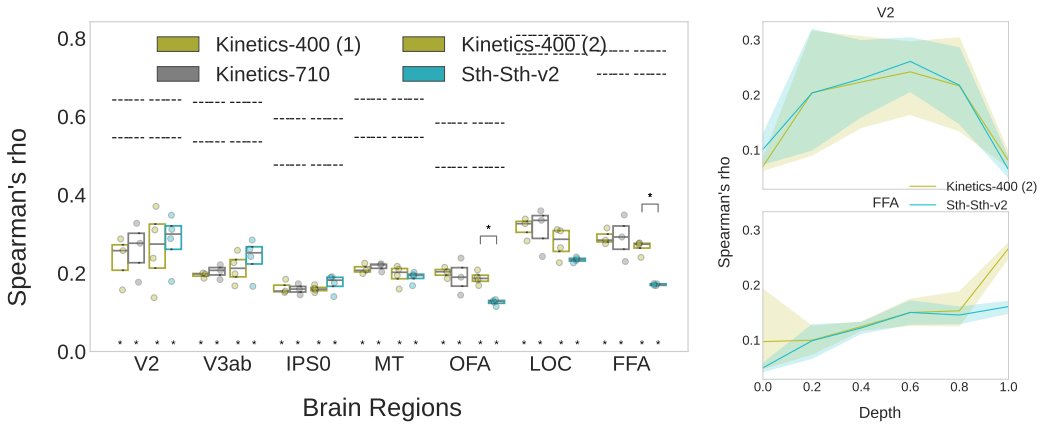

(a) (b)

Figure 5: **Varying the training dataset:** Training dataset biases transfer to alignment with functionally selective brain areas. We compare the same three models trained on Kinetics 400 and Kinetics 710, and the same four models trained on Kinetics 400 and Something-Something-v2. Models trained on Kinetics 400 are numbered as (1) and (2) to indicate two different sets of models compared with Kinetics 710 and Something-Something-v2 respectively, and the comparisons are also separated with a gap. In 5a the highest-scoring layers are shown, selecting a representative sample of regions (the rest in Appendix C), and in 5b we zoom in on two regions to show all layer depths.

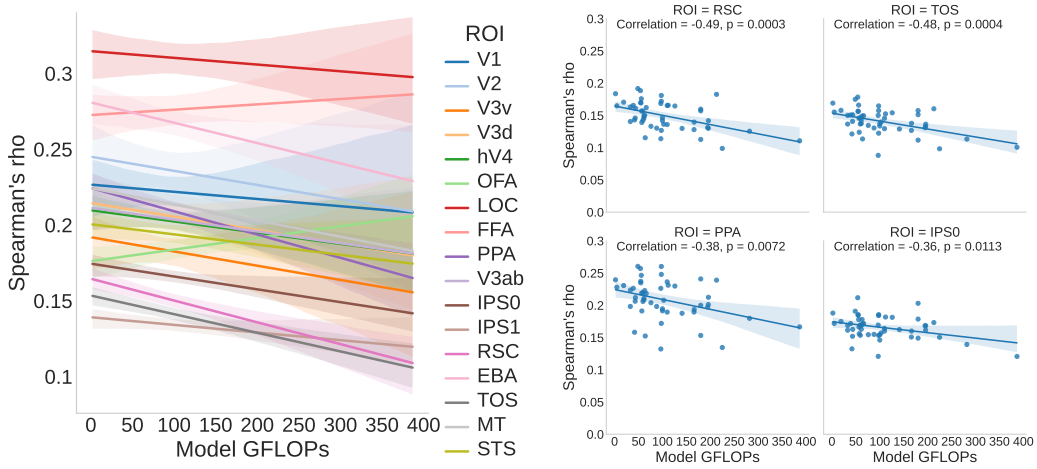

(a) (b)

Figure 6: **Relation to computational complexity:** We show a significant negative correlation of model FLOPs to alignment in several high-level brain areas. We correlate the RSA scores of video models to model FLOPs, using the best RSA scoring layer for each model and report all brain regions (6a), as well as highlight those with the most significant correlations (6b).

5 Discussion

Decoupling the role of temporal modeling and action space optimization. For alignment of video models to brains watching videos, different factors affect model-brain alignment at different stages of visual processing. In early areas, temporal modeling improves alignment, while optimizing for action recognition does not. The latter on its own can even result in slightly worse alignment than object recognition models, hinting to a potential degradation of low-level features during action optimization (image action recognition models are pretrained on ImageNet first). The benefit of temporal modeling for alignment with early brain areas is consistent with neuroscience literature suggesting that these areas are more sensitive to short time-scale change in the input, while late areas are more temporally invariant (Hasson et al., 2008; Groen et al., 2022; Brands et al., 2024). There, improvement over object recognition image models only comes from optimizing for action recognition and is only reflected in the models' classification layer. This could mean (1) that the information captured in late brain areas is dominated by semantics and particularly action categories (Lahner et al., 2024). Or (2) that current state-of-the-art video models fail to capture the more

fine-grained high level video representations present in the brain, aside from action labels. Future work is needed to resolve these competing accounts. In line with (Mineault et al., 2021), we find no indication that action information affects alignment more for areas involved in navigation such as RSC or motion area MT. Garcia et al. (2024) observed a different patttern of results from ours, finding improved alignment for video models in Lateral ROIs only. This could reflect methodological differences (e.g. fMRI dataset, dimensionality reduction method, brain alignment metric). Our findings are consistent with a recent video reconstruction study (Lu et al., 2024a) which shows that intermediate and late regions contribute more to the decoding of video semantics, while early areas more to the decoding of low-level structure and motion in the videos.

Comparing early and late representations of CNNs and Transformers. CNNs exhibit a better hierarchy overall, as there is a clear mid-depth peak for early regions and gradual improvement as depth increases for late regions. Transformers however achieve an impressive correlation to early regions even from one tenth of layer depth. This also holds for image CNNs and Transformers (Appendix D). Conwell et al. (2022) did not comment on these interesting nuances as layer-wise comparisons were not performed. Why would Transformers have more human-aligned representations earlier in the network than CNNs? While early visual areas are known to process information locally (similar to CNNs), the global attention in Transformers could, from an earlier layer, better capture the representations in those areas. Indeed, Raghu et al. (2021) showed that representations in layers 0-60 of a CNN are more similar to layers 0-30 of a Transformer, and CNN layers 60-120 more similar to Transformer layers 30-140. Transformers also exhibited more stable representations across layers, while CNNs showed a clear divide between early and late layers. In Tuli et al. (2021), error patterns of Transformers were more similar to human than those of CNNs, indicating a higher behavioral alignment - we find that alignment in high-level areas based on semantic representations is mostly equivalent across both architectures. In future work it is also worth investigating hybrid models (e.g. Transformers using both convolution and self-attention), as there are indications these might achieve a balance between the two architectures (Appendix D).

Relating training biases and computational efficiency to alignment. Our comparison of brain alignment between models trained on different action datasets shows that dataset biases related to a certain functional selectivity can be transferred in brain alignment with the respective functionally selective brain area. This highlights the importance of choosing models trained on a dataset that is representative (1) of the videos humans watch in the experiment, and (2) of the hypotheses tested when measuring alignment. Our observation that computationally expensive models are less aligned to higher brain areas leads us to conclude that human-like semantics are more achievable with computationally efficient models. This is important for machine learning research that aims to build increasingly efficient models for increasingly complex tasks, as it is an indication that more computational resources may not be needed to compute human-like high-level representations. Ideas in this direction include using the top-aligned models as starting points for further component ablations towards alignment and efficiency, as well as pruning models to preserve alignment.

Limitations and future work. We base our choice of alignment metric on the comparison of RSA and veRSA made in Conwell et al. (2022), but this was on static images and it could be worthwhile to make the same comparison for our video data, as well as comparison between other metrics. RSA does not examine possible gains in predictivity as a result of linear feature re-weighting. Next, we benchmark video models that are part of a library and not all publicly available video models, which limits the comparisons we could make; to show a controlled comparison of learning paradigms we would need multiples of the same architecture in supervised, contrastive, and self-supervised variants. Our results are based on a single fMRI dataset, and not validated across multiple fMRI experimental setups. BOLD signals are also indirect measurements of brain activity, which in turn is an indirect measurement of the brain's representations - these are latent variables that cannot be measured. Our fMRI analyses were conducted in volume space; surface-based analysis could potentially provide better predictions of brain function (Glasser et al., 2016; Coalson et al., 2018). Importantly, fMRI lacks good temporal resolution which is crucial to investigate temporal modeling at finer detail. Future steps in that direction would be to make use of all temporal samples available in the fMRI data (3 TRs) and collection of EEG/MEG data for the same videos, to perform alignment benchmarking jointly on fMRI and EEG/MEG - our work sets the foundations for such future studies by already uncovering differences in models performing temporal modeling with fMRI. Given that motion and imagery cues in videos likely also engage non-visual brain regions, another promising direction for future work is to study representational alignment in areas outside visual cortex.

REFERENCES

Emily J Allen, Ghislain St-Yves, Yihan Wu, Jesse L Breedlove, Jacob S Prince, Logan T Dowdle, Matthias Nau, Brad Caron, Franco Pestilli, Ian Charest, et al. A massive 7t fmri dataset to bridge cognitive neuroscience and artificial intelligence. *Nature neuroscience*, 25(1):116–126, 2022.

Alex Andonian, Camilo Fosco, Mathew Monfort, Allen Lee, Rogerio Feris, Carl Vondrick, and Aude Oliva. We have so much in common: Modeling semantic relational set abstractions in videos. In *Computer Vision–ECCV 2020: 16th European Conference, Glasgow, UK, August 23–28, 2020, Proceedings, Part XVIII 16*, pp. 18–34. Springer, 2020.

Clemens G Bartnik, Christina Sartzetaki, Abel Puigsesslloses Sanchez, Elijah Molenkamp, Steven Bommer, Nikolina Vukšić, and Iris IA Groen. Distinct representation of locomotive action affordances in human behavior, brains and deep neural networks. *bioRxiv*, pp. 2024–05, 2024.

Domenic Bersch, Kshitij Dwivedi, Martina Vilas, Radoslaw M Cichy, and Gemma Roig. Net2brain: A toolbox to compare artificial vision models with human brain responses. *arXiv preprint arXiv:2208.09677*, 2022.

Amber Marijn Brands, Sasha Devore, Orrin Devinsky, Werner Doyle, Adeen Flinker, Daniel Friedman, Patricia Dugan, Jonathan Winawer, and Iris Isabelle Anna Groen. Temporal dynamics of short-term neural adaptation across human visual cortex. *PLOS Computational Biology*, 20(5): e1012161, 2024.

Joao Carreira and Andrew Zisserman. Quo vadis, action recognition? a new model and the kinetics dataset. In *proceedings of the IEEE Conference on Computer Vision and Pattern Recognition*, pp. 6299–6308, 2017.

Joao Carreira, Eric Noland, Chloe Hillier, and Andrew Zisserman. A short note on the kinetics-700 human action dataset. *arXiv preprint arXiv:1907.06987*, 2019.

Radoslaw Martin Cichy, Aditya Khosla, Dimitrios Pantazis, Antonio Torralba, and Aude Oliva. Comparison of deep neural networks to spatio-temporal cortical dynamics of human visual object recognition reveals hierarchical correspondence. *Scientific reports*, 6(1):27755, 2016.

Radoslaw Martin Cichy, Gemma Roig, Alex Andonian, Kshitij Dwivedi, Benjamin Lahner, Alex Lascelles, Yalda Mohsenzadeh, Kandan Ramakrishnan, and Aude Oliva. The algonauts project: A platform for communication between the sciences of biological and artificial intelligence. *arXiv preprint arXiv:1905.05675*, 2019.

Radoslaw Martin Cichy, Kshitij Dwivedi, Benjamin Lahner, Alex Lascelles, Polina Iamshchinina, Monika Graumann, Alex Andonian, NAR Murty, K Kay, Gemma Roig, et al. The algonauts project 2021 challenge: How the human brain makes sense of a world in motion. *arXiv preprint arXiv:2104.13714*, 2021.

Timothy S Coalson, David C Van Essen, and Matthew F Glasser. The impact of traditional neuroimaging methods on the spatial localization of cortical areas. *Proceedings of the National Academy of Sciences*, 115(27):E6356–E6365, 2018.

Colin Conwell, Jacob S Prince, Kendrick N Kay, George A Alvarez, and Talia Konkle. What can 1.8 billion regressions tell us about the pressures shaping high-level visual representation in brains and machines? *BioRxiv*, pp. 2022–03, 2022.

Jody Culham, Sheng He, Sean Dukelow, and Frans AJ Verstraten. Visual motion and the human brain: what has neuroimaging told us? *Acta psychologica*, 107(1-3):69–94, 2001.

Diana C Dima, Tyler M Tomita, Christopher J Honey, and Leyla Isik. Social-affective features drive human representations of observed actions. *Elife*, 11:e75027, 2022.

Katharina Dobs, Leyla Isik, Dimitrios Pantazis, and Nancy Kanwisher. How face perception unfolds over time. *Nature communications*, 10(1):1258, 2019.

Adrien Doerig, Rowan P Sommers, Katja Seeliger, Blake Richards, Jenann Ismael, Grace W Lindsay, Konrad P Kording, Talia Konkle, Marcel AJ Van Gerven, Nikolaus Kriegeskorte, et al. The neuroconnectionist research programme. *Nature Reviews Neuroscience*, 24(7):431–450, 2023.

Kshitij Dwivedi, Michael F Bonner, Radoslaw Martin Cichy, and Gemma Roig. Unveiling functions of the visual cortex using task-specific deep neural networks. *PLoS computational biology*, 17(8): e1009267, 2021.

Stéphane d'Ascoli, Hugo Touvron, Matthew L Leavitt, Ari S Morcos, Giulio Biroli, and Levent Sagun. Convit: Improving vision transformers with soft convolutional inductive biases. In *International conference on machine learning*, pp. 2286–2296. PMLR, 2021.

Michael Eickenberg, Alexandre Gramfort, Gaël Varoquaux, and Bertrand Thirion. Seeing it all: Convolutional network layers map the function of the human visual system. *NeuroImage*, 152: 184–194, 2017.

Oscar Esteban, Christopher J Markiewicz, Ross W Blair, Craig A Moodie, A Ilkay Isik, Asier Erramuzpe, James D Kent, Mathias Goncalves, Elizabeth DuPre, Madeleine Snyder, et al. fmriprep: a robust preprocessing pipeline for functional mri. *Nature methods*, 16(1):111–116, 2019.

Christoph Feichtenhofer, Haoqi Fan, Jitendra Malik, and Kaiming He. Slowfast networks for video recognition. In *Proceedings of the IEEE/CVF international conference on computer vision*, pp. 6202–6211, 2019.

Kathy Garcia, Emalie McMahon, Colin Conwell, Michael F Bonner, and Leyla Isik. Modeling dynamic social vision highlights gaps between deep learning and humans. *PsyArXiv*, 2024.

Alessandro T Gifford, Benjamin Lahner, Sari Saba-Sadiya, Martina G Vilas, Alex Lascelles, Aude Oliva, Kendrick Kay, Gemma Roig, and Radoslaw M Cichy. The algonauts project 2023 challenge: How the human brain makes sense of natural scenes. *arXiv preprint arXiv:2301.03198*, 2023.

Matthew F Glasser, Timothy S Coalson, Emma C Robinson, Carl D Hacker, John Harwell, Essa Yacoub, Kamil Ugurbil, Jesper Andersson, Christian F Beckmann, Mark Jenkinson, et al. A multi-modal parcellation of human cerebral cortex. *Nature*, 536(7615):171–178, 2016.

Raghav Goyal, Samira Ebrahimi Kahou, Vincent Michalski, Joanna Materzynska, Susanne Westphal, Heuna Kim, Valentin Haenel, Ingo Fruend, Peter Yianilos, Moritz Mueller-Freitag, et al. The" something something" video database for learning and evaluating visual common sense. In *Proceedings of the IEEE international conference on computer vision*, pp. 5842–5850, 2017.

Kalanit Grill-Spector and Rafael Malach. The human visual cortex. *Annu. Rev. Neurosci.*, 27(1): 649–677, 2004.

Iris IA Groen, Giovanni Piantoni, Stephanie Montenegro, Adeen Flinker, Sasha Devore, Orrin Devinsky, Werner Doyle, Patricia Dugan, Daniel Friedman, Nick F Ramsey, et al. Temporal dynamics of neural responses in human visual cortex. *Journal of Neuroscience*, 42(40):7562–7580, 2022.

Umut Güçlü and Marcel AJ Van Gerven. Deep neural networks reveal a gradient in the complexity of neural representations across the ventral stream. *Journal of Neuroscience*, 35(27):10005–10014, 2015.

Uri Hasson, Eunice Yang, Ignacio Vallines, David J Heeger, and Nava Rubin. A hierarchy of temporal receptive windows in human cortex. *Journal of neuroscience*, 28(10):2539–2550, 2008.

Martin N Hebart, Oliver Contier, Lina Teichmann, Adam H Rockter, Charles Y Zheng, Alexis Kidder, Anna Corriveau, Maryam Vaziri-Pashkam, and Chris I Baker. Things-data, a multimodal collection of large-scale datasets for investigating object representations in human brain and behavior. *Elife*, 12:e82580, 2023.

Joshua B Julian, Evelina Fedorenko, Jason Webster, and Nancy Kanwisher. An algorithmic method for functionally defining regions of interest in the ventral visual pathway. *Neuroimage*, 60(4): 2357–2364, 2012.

Will Kay, Joao Carreira, Karen Simonyan, Brian Zhang, Chloe Hillier, Sudheendra Vijayanarasimhan, Fabio Viola, Tim Green, Trevor Back, Paul Natsev, et al. The kinetics human action video dataset. *arXiv preprint arXiv:1705.06950*, 2017.

Seyed-Mahdi Khaligh-Razavi, Linda Henriksson, Kendrick Kay, and Nikolaus Kriegeskorte. Fixed versus mixed rsa: Explaining visual representations by fixed and mixed feature sets from shallow and deep computational models. *Journal of Mathematical Psychology*, 76:184–197, 2017.

Marcie L King, Iris IA Groen, Adam Steel, Dwight J Kravitz, and Chris I Baker. Similarity judgments and cortical visual responses reflect different properties of object and scene categories in naturalistic images. *NeuroImage*, 197:368–382, 2019.

Talia Konkle and George A Alvarez. A self-supervised domain-general learning framework for human ventral stream representation. *Nature communications*, 13(1):491, 2022.

Dwight J Kravitz, Kadharbatcha S Saleem, Chris I Baker, and Mortimer Mishkin. A new neural framework for visuospatial processing. *Nature Reviews Neuroscience*, 12(4):217–230, 2011.

Nikolaus Kriegeskorte and Pamela K Douglas. Cognitive computational neuroscience. *Nature neuroscience*, 21(9):1148–1160, 2018.

Nikolaus Kriegeskorte, Marieke Mur, and Peter A Bandettini. Representational similarity analysis-connecting the branches of systems neuroscience. *Frontiers in systems neuroscience*, 2:249, 2008.

Emel Küçük, Matthew Foxwell, Daniel Kaiser, and David Pitcher. Moving and static faces, bodies, objects, and scenes are differentially represented across the three visual pathways. *Journal of Cognitive Neuroscience*, pp. 1–13, 2024.

Tom Dupré La Tour, Michael Eickenberg, Anwar O Nunez-Elizalde, and Jack L Gallant. Feature-space selection with banded ridge regression. *NeuroImage*, 264:119728, 2022.

Benjamin Lahner, Kshitij Dwivedi, Polina Iamshchinina, Monika Graumann, Alex Lascelles, Gemma Roig, Alessandro Thomas Gifford, Bowen Pan, SouYoung Jin, N Apurva Ratan Murty, et al. Modeling short visual events through the bold moments video fmri dataset and metadata. *Nature communications*, 15(1):6241, 2024.

Kunchang Li, Yali Wang, Peng Gao, Guanglu Song, Yu Liu, Hongsheng Li, and Yu Qiao. Uniformer: Unified transformer for efficient spatiotemporal representation learning. *arXiv preprint arXiv:2201.04676*, 2022.

Kunchang Li, Yali Wang, Yinan He, Yizhuo Li, Yi Wang, Limin Wang, and Yu Qiao. Uniformerv2: Unlocking the potential of image vits for video understanding. In *Proceedings of the IEEE/CVF International Conference on Computer Vision*, pp. 1632–1643, 2023a.

Kunchang Li, Yali Wang, Junhao Zhang, Peng Gao, Guanglu Song, Yu Liu, Hongsheng Li, and Yu Qiao. Uniformer: Unifying convolution and self-attention for visual recognition. *IEEE Transactions on Pattern Analysis and Machine Intelligence*, 45(10):12581–12600, 2023b.

Ji Lin, Chuang Gan, and Song Han. Tsm: Temporal shift module for efficient video understanding. In *Proceedings of the IEEE/CVF international conference on computer vision*, pp. 7083–7093, 2019.

Ze Liu, Jia Ning, Yue Cao, Yixuan Wei, Zheng Zhang, Stephen Lin, and Han Hu. Video swin transformer. In *Proceedings of the IEEE/CVF conference on computer vision and pattern recognition*, pp. 3202–3211, 2022.

Yizhuo Lu, Changde Du, Chong Wang, Xuanliu Zhu, Liuyun Jiang, and Huiguang He. Animate your thoughts: Decoupled reconstruction of dynamic natural vision from slow brain activity. *arXiv preprint arXiv:2405.03280*, 2024a.

Zitong Lu, Yile Wang, and Julie D Golomb. Achieving more human brain-like vision via human eeg representational alignment. *ArXiv*, 2024b.

Raja Marjieh, Pol Van Rijn, Ilia Sucholutsky, Theodore Sumers, Harin Lee, Thomas L. Griffiths, and Nori Jacoby. Words are all you need? language as an approximation for human similarity judgments. In *The Eleventh International Conference on Learning Representations*, 2023. URL https://openreview.net/forum?id=O-G91-4cMdv.

Emalie McMahon, Michael F Bonner, and Leyla Isik. Hierarchical organization of social action features along the lateral visual pathway. *Current Biology*, 33(23):5035–5047, 2023.

Juliette Millet, Charlotte Caucheteux, Yves Boubenec, Alexandre Gramfort, Ewan Dunbar, Christophe Pallier, Jean-Remi King, et al. Toward a realistic model of speech processing in the brain with self-supervised learning. *Advances in Neural Information Processing Systems*, 35: 33428–33443, 2022.

Patrick Mineault, Shahab Bakhtiari, Blake Richards, and Christopher Pack. Your head is there to move you around: Goal-driven models of the primate dorsal pathway. *Advances in Neural Information Processing Systems*, 34:28757–28771, 2021.

Mortimer Mishkin, Leslie G Ungerleider, and Kathleen A Macko. Object vision and spatial vision: two cortical pathways. *Trends in neurosciences*, 6:414–417, 1983.

Mathew Monfort, Alex Andonian, Bolei Zhou, Kandan Ramakrishnan, Sarah Adel Bargal, Tom Yan, Lisa Brown, Quanfu Fan, Dan Gutfreund, Carl Vondrick, et al. Moments in time dataset: one million videos for event understanding. *IEEE transactions on pattern analysis and machine intelligence*, 42(2):502–508, 2019.

Mathew Monfort, Bowen Pan, Kandan Ramakrishnan, Alex Andonian, Barry A McNamara, Alex Lascelles, Quanfu Fan, Dan Gutfreund, Rogério Schmidt Feris, and Aude Oliva. Multi-moments in time: Learning and interpreting models for multi-action video understanding. *IEEE Transactions on Pattern Analysis and Machine Intelligence*, 44(12):9434–9445, 2021.

Lukas Muttenthaler, Jonas Dippel, Lorenz Linhardt, Robert A. Vandermeulen, and Simon Kornblith. Human alignment of neural network representations. In *The Eleventh International Conference on Learning Representations*, 2023. URL https://openreview.net/forum?id=ReDQ1OUQR0X.

Hamed Nili, Cai Wingfield, Alexander Walther, Li Su, William Marslen-Wilson, and Nikolaus Kriegeskorte. A toolbox for representational similarity analysis. *PLoS computational biology*, 10(4):e1003553, 2014.

David Pitcher and Leslie G Ungerleider. Evidence for a third visual pathway specialized for social perception. *Trends in cognitive sciences*, 25(2):100–110, 2021.

Jacob S Prince, Ian Charest, Jan W Kurzawski, John A Pyles, Michael J Tarr, and Kendrick N Kay. Improving the accuracy of single-trial fmri response estimates using glmsingle. *Elife*, 11:e77599, 2022.

Maithra Raghu, Thomas Unterthiner, Simon Kornblith, Chiyuan Zhang, and Alexey Dosovitskiy. Do vision transformers see like convolutional neural networks? *Advances in neural information processing systems*, 34:12116–12128, 2021.

Martin Schrimpf, Jonas Kubilius, Ha Hong, Najib J Majaj, Rishi Rajalingham, Elias B Issa, Kohitij Kar, Pouya Bashivan, Jonathan Prescott-Roy, Franziska Geiger, et al. Brain-score: Which artificial neural network for object recognition is most brain-like? *BioRxiv*, pp. 407007, 2018.

Martin Schrimpf, Jonas Kubilius, Michael J Lee, N Apurva Ratan Murty, Robert Ajemian, and James J DiCarlo. Integrative benchmarking to advance neurally mechanistic models of human intelligence. *Neuron*, 108(3):413–423, 2020.

Robert Sekuler, Scott NJ Watamaniuk, and Randolph Blake. Motion perception. *Steven's Handbook of Experimental Psychology*, 1:121–176, 2002.

Karen Simonyan and Andrew Zisserman. Two-stream convolutional networks for action recognition in videos. *Advances in neural information processing systems*, 27, 2014.

Ghislain St-Yves and Thomas Naselaris. The feature-weighted receptive field: an interpretable encoding model for complex feature spaces. *NeuroImage*, 180:188–202, 2018.

Ilia Sucholutsky, Lukas Muttenthaler, Adrian Weller, Andi Peng, Andreea Bobu, Been Kim, Bradley C Love, Erin Grant, Jascha Achterberg, Joshua B Tenenbaum, et al. Getting aligned on representational alignment. *arXiv preprint arXiv:2310.13018*, 2023.

Du Tran, Lubomir Bourdev, Rob Fergus, Lorenzo Torresani, and Manohar Paluri. Learning spatiotemporal features with 3d convolutional networks. In *Proceedings of the IEEE international conference on computer vision*, pp. 4489–4497, 2015.

Shikhar Tuli, Ishita Dasgupta, Erin Grant, and Thomas L Griffiths. Are convolutional neural networks or transformers more like human vision? *arXiv preprint arXiv:2105.07197*, 2021.

Alexander Walther, Hamed Nili, Naveed Ejaz, Arjen Alink, Nikolaus Kriegeskorte, and Jörn Diedrichsen. Reliability of dissimilarity measures for multi-voxel pattern analysis. *Neuroimage*, 137:188–200, 2016.

Aria Y Wang, Kendrick Kay, Thomas Naselaris, Michael J Tarr, and Leila Wehbe. Better models of human high-level visual cortex emerge from natural language supervision with a large and diverse dataset. *Nature Machine Intelligence*, 5(12):1415–1426, 2023a.

Liang Wang, Ryan EB Mruczek, Michael J Arcaro, and Sabine Kastner. Probabilistic maps of visual topography in human cortex. *Cerebral cortex*, 25(10):3911–3931, 2015.

Limin Wang, Bingkun Huang, Zhiyu Zhao, Zhan Tong, Yinan He, Yi Wang, Yali Wang, and Yu Qiao. Videomae v2: Scaling video masked autoencoders with dual masking. In *Proceedings of the IEEE/CVF Conference on Computer Vision and Pattern Recognition*, pp. 14549–14560, 2023b.

Bolei Zhou, Alex Andonian, Aude Oliva, and Antonio Torralba. Temporal relational reasoning in videos. In *Proceedings of the European conference on computer vision (ECCV)*, pp. 803–818, 2018a.

Jingyang Zhou, Noah C Benson, Kendrick N Kay, and Jonathan Winawer. Compressive temporal summation in human visual cortex. *Journal of Neuroscience*, 38(3):691–709, 2018b.

Ming Zhou, Zhengxin Gong, Yuxuan Dai, Yushan Wen, Youyi Liu, and Zonglei Zhen. A large-scale fmri dataset for human action recognition. *Scientific Data*, 10(1):415, 2023.

APPENDIX

A BRAIN DATASET DETAILS

Below, we provide a summary of the Methods section of the BMD dataset Lahner et al. (2024).

Participants Ten healthy volunteers (6 female, mean age ± SD = 27.01 ± 3.96 years, sex self-reported) with normal or corrected-to-normal vision participated in the experiment. All participants gave informed consent and were screened for MRI safety. The experiment was conducted in accordance with the Declaration of Helsinki and approved by the local ethics committee.

Stimuli The stimulus set consisted of 1102 videos in total and were sampled from the Memento10k dataset41. Each video was square-cropped and resized to 268×268 pixels. Videos had a duration of 3 s and frame rates ranging from 15 to 30 frames per second. Videos were manually selected from the Memento10k dataset by two human observers to encompass videos that contained movement (i.e., no static content), were filmed in a natural context, and represented a wide selection of possible events a human might witness. The 1102 videos selected for the main experiment were split into a training and a testing set; 102 videos were randomly chosen for the testing set. Subjects additionally viewed a separate set of colored, naturalistic videos (18 s length, composed of 6 3-second videos) corresponding to one of five categories (faces, bodies, scenes, objects, and scrambled objects) in order to functionally localize each subject's category selective regions of interest (ROIs, see below).

MRI data acquisition The MRI data were acquired with a 3 T Trio Siemens scanner using a 32-channel head coil. During the experimental runs, functional T2*-weighted gradient-echo echo-planar images (EPI) were collected (TR = 1750 ms, TE = 30 ms, flip angle = 71°, FOV read = 190 mm, FOV phase = 100%, bandwidth = 2268 Hz/Px, resolution = 2.5 × 2.5 × 2.5 mm, slice gap = 10%, slices = 54, multi-band acceleration factor = 2, ascending interleaved acquisition). Additionally, a structural T1-weighted image (TR = 1900 ms, TE = 2.52 ms, flip angle = 9°, FOV read = 256 mm, FOV phase = 100%, bandwidth = 170 Hz/px, resolution = 1.0 × 1.0 × 1.0 mm, slices = 176 sagittal slices, multi-slice mode = single shot, ascending) and T2-weighted image (TR = 7970 ms, TE = 120 ms, flip angle = 90°, FOV read = 256 mm, FOV phase = 100%, bandwidth = 362 Hz/Px, resolution = 1.0 × 1.0 × 1.1 mm, slice gap = 10%, slices = 128, multi-slice mode = interleaved, scending) were obtained as high-resolution anatomical references. Dual echo fieldmaps (TR = 636 ms, TE1 = 5.72 ms, TE2 = 8.18 ms, flip angle = 60°, FOV read = 190 mm, FOV phase = 100%, bandwidth = 260 Hz/Px, resolution = 2.5 × 2.5 × 2.5 mm, slice gap = 10%, slices = 54, ascending interleaved acquisition) were acquired at the beginning of every session to post-hoc correct for spatial distortion of functional scans induced by magnetic field inhomogeneities. Subjects completed a total of 5 separate fMRI sessions on separate days. Session 1 consisted of structural scans, functional localizer runs, and functional resting state scans all interspersed. Sessions 2–5 consisted of the main functional experimental runs where the subjects viewed the training and testing set videos.

MRI data preprocessing Raw MRI data was converted to BIDS format63 and preprocessed using the standardized fMRIPrep preprocessing pipeline (Esteban et al., 2019). Lahner et al. (2024) provide preprocessed data from two different pipelines, with MRI activations in Version A being calculated using Finite Impulse Response estimates, while Version B uses GLMsingle (Prince et al., 2022). We use Version B, as the authors recommend it for being higher quality. The full fMRIPrep-generated preprocessing report is found in (Lahner et al., 2024). Briefly, it consisted of anatomical data preprocessing (intensity non-uniformity correction, skull-stripping, surface segmentation, and volume-based spatial registration to standard MNI152N-Lin2009cAsym space) and functional data preprocessing (B0-nonuniformity correction, head-motion estimation, slice-time correction, and registration to the anatomical reference, with all spatial transformations concatenated into a single step), generating preprocessed BOLD runs in standard MNI space. Functional localizer scans were spatially smoothed (9 mm FWHM) while the main experimental data remained unsmoothed.

Brain response estimation A General Linear Model (GLM) was used to estimate single-trial beta estimates for each video. First, the main experimental runs were temporally interpolated from their acquisition TR of 1.75 seconds to a TR of 1 second to time-lock volume sampling to stimulus presentations. The interpolated fMRI time series, stimulus onsets, and stimulus durations (modeled with 3s durations) for each session separately were input to GLMsingle (Prince et al., 2022), which estimates single-trial beta values by (1) fitting an optimal Hemodynamic Response Function (HRF) to each voxel from a library of HRFs, (2) identifying nuisance regressors from a noise pool that

maximally explain variance, and (3) implementing fractional ridge regression to improve estimates in a rapid event-related design. The resulting single-trial beta estimates were normalized within each scanning session using the session's training set mean and standard deviation.

ROI definitions A set of 23 ROIs (each separated by left and right hemispheres) previously known to be driven by dynamic stimuli spanning visual and parietal cortices were defined by (Lahner et al., 2024) by creating a non-overlapping parcellation composed of parcels resampled from several anatomical atlases (Glasser et al., 2016; Wang et al., 2015; Julian et al., 2012), into standard MNI152NLin2009cAsym space. Then, brain activations estimated from the independent functional localizer runs were used to identify the top 50% of activated voxels within each of the corresponding parcels. This ROI definition method facilitates inter-subject modeling by ensuring all ROIs were defined for each subject and each ROI contained the same number of voxels across subjects. The defined ROIs were V1v, V1d, V2v, V2d, V3v, V3d, hV4, V3ab, IPS0, IPS1-3, BA2, 7AL, PFt, PFop, and MT, EBA, LOC, PPA, RSC, STS, OFA, FFA, and STS, separately for each hemisphere.

B IMPLEMENTATION DETAILS

Table 2: Exhaustive account of all models benchmarked.

Image Object Recognition		**Action Recognition**	
CNNs	**Transformers**	**CNNs**	**Transformers**
AlexNet	CAiT_S	IR_CSN_R152	MViTv2_S[b]
DenseNet161	CAiT_XXS	IR_CSN_R152_BNfrozen_IG65M	MViTv2_B[b]
DenseNet201	ConViT_S	IR_CSN_R50_BNfrozen_IG65M	TimeSformer_DivST
EfficientNetB3	ConViT_B	IR_CSN_R152_IG65M	TimeSformer_JointST
EfficientNetB6	DEiT_S	IP_CSN_R152_IG65M	Uniformer_S
RegNetX16gf	DEiT_B	IP_CSN_R152	Uniformer_B
RegNetY8gf	MViTv2_S	I3D_R50	Uniformerv2_B[a]
ResNet34	MViTv2_B	I3D_R50_dotprod	Uniformerv2_B_k710pre
ResNet50	Swin_T	I3D_R50_embgauss	VideoMAE_B
ResNet101	Swin_S	I3D_R50_gauss	VideoMAEv2_S
ResNet152	Swin_B	I3D_R50_heavy	VideoMAEv2_S
ResNeXt50	Twins_pcpvt_B	R2P1D_R50	VideoSwin_T
ResNeXt101	ViT_S	SlowFast_R50	VideoSwin_S[a]
VGG11	ViT_B	SlowFast_R101	VideoSwin_B
VGG11BN		Slow_R50	
VGG19		Slow_R101	
VGG19BN		Slow_R50_IN1k[a]	
WideResNet50		Slow_R50_IN1k_embgauss	
WideResNet101		TaNet_R50	
InceptionV3		TPN_R50	
InceptionV4		TSM_R50[b]	
RepVGGa2		TSM_R50_dotprod	
RepVGGb2		TSM_R50_embgauss	
SeResNet50		TSM_R50_gauss	
SeResNeXt50		TSM_MobOne_s4	
Xception41		X3D_S	
Xception71		X3D_M	
		C2D_R50_nopool	TimeSformer_SpaceOnly
		C2D_R101_nopool	TSN_Swin
		C2D_R50_pool8	
		C2D_R50_pool16	
		TSN_R50[b]	
		TSN_R101	
		TSN_D161	
		TSN_MobOne_s4	

[a] Availability also on Kinetics 710 (Carreira et al., 2019)
[b] Availability also on Something-Something-v2 (Goyal et al., 2017)

For parts of our pipeline for RSA, we make use of the Net2Brain python library (Bersch et al., 2022).

C ALL REGIONS OF INTEREST

In this section we exhibit all Regions of Interest (ROIs) for analyses where a subset of the ROIs was shown in the main results.

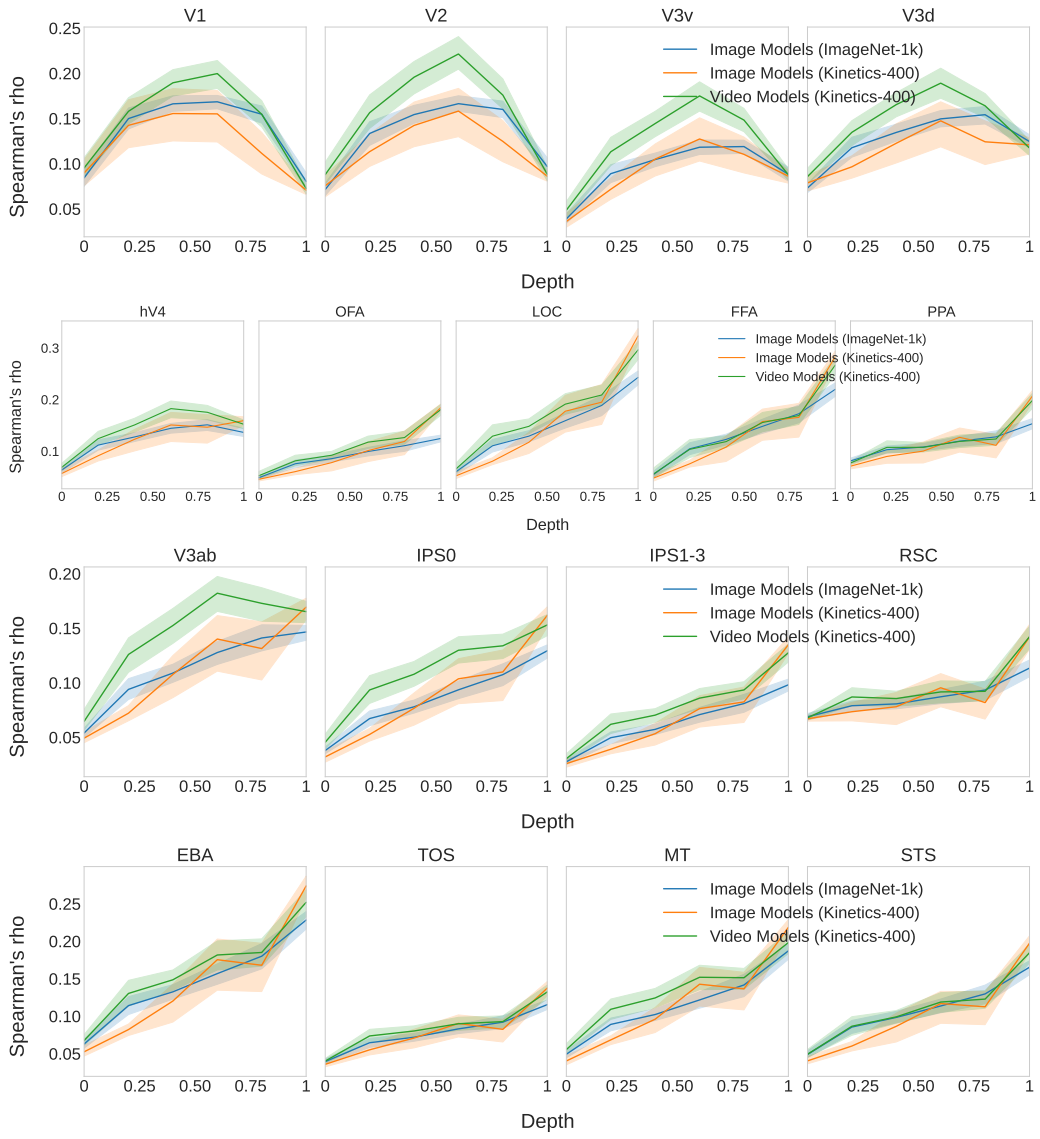

Figure 7: Expanding figure 2b to show for all ROIs the comparison across layers of object recognition image models and action recognition image and video models.

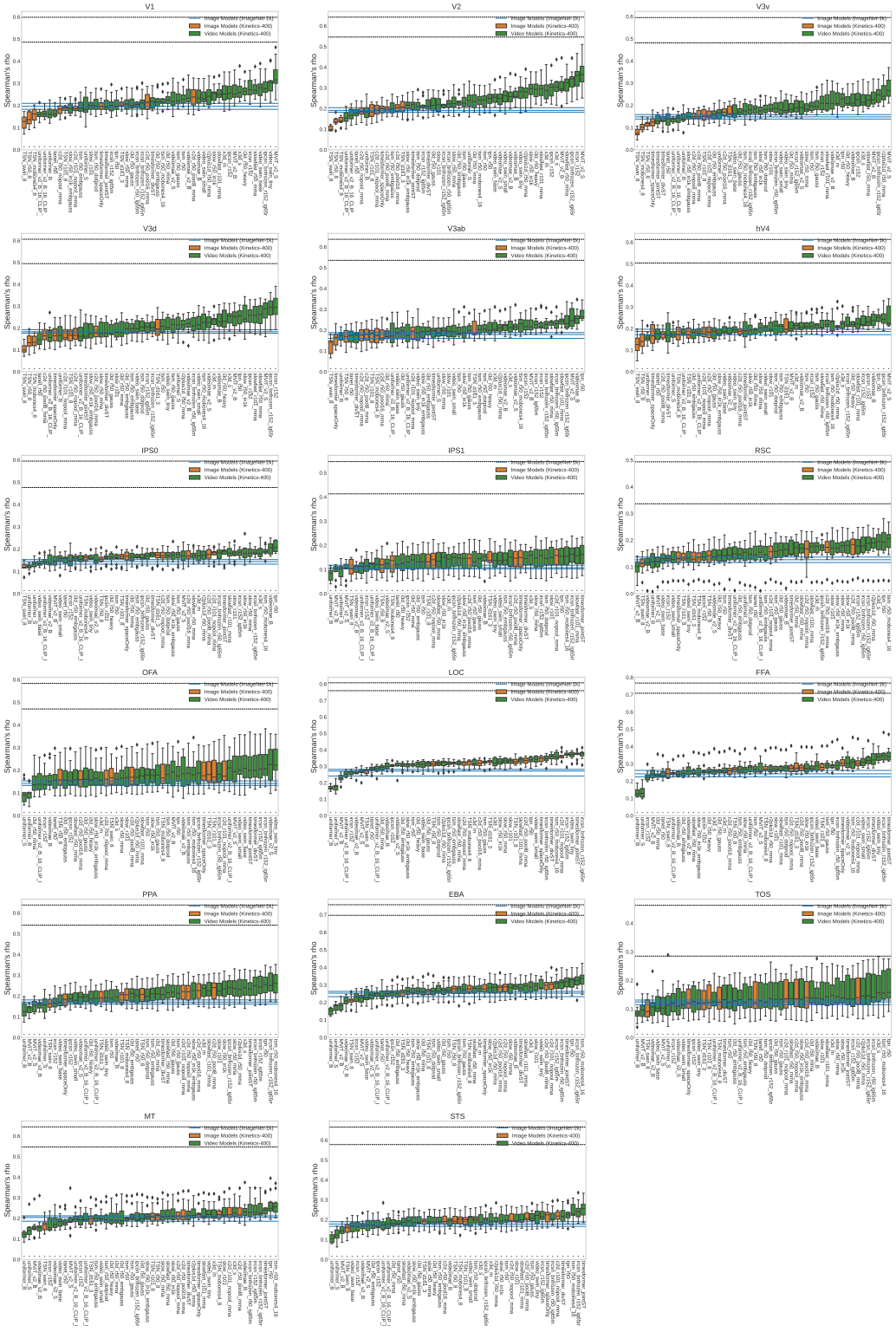

Figure 8: Expanding figure 3 to show model ranking for all ROIs.

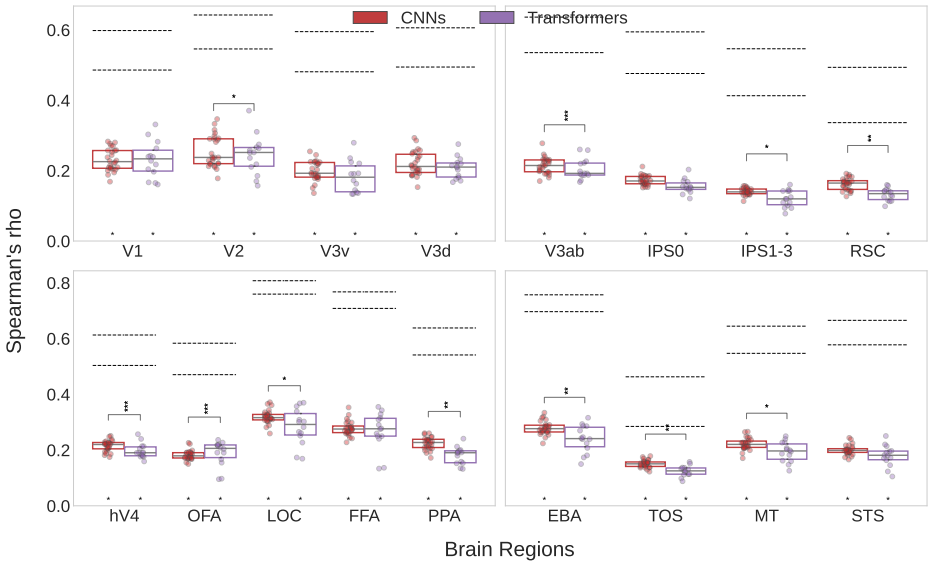

Figure 9: Expanding figure 4a to show all ROIs for the comparison of CNNs and Transformers.

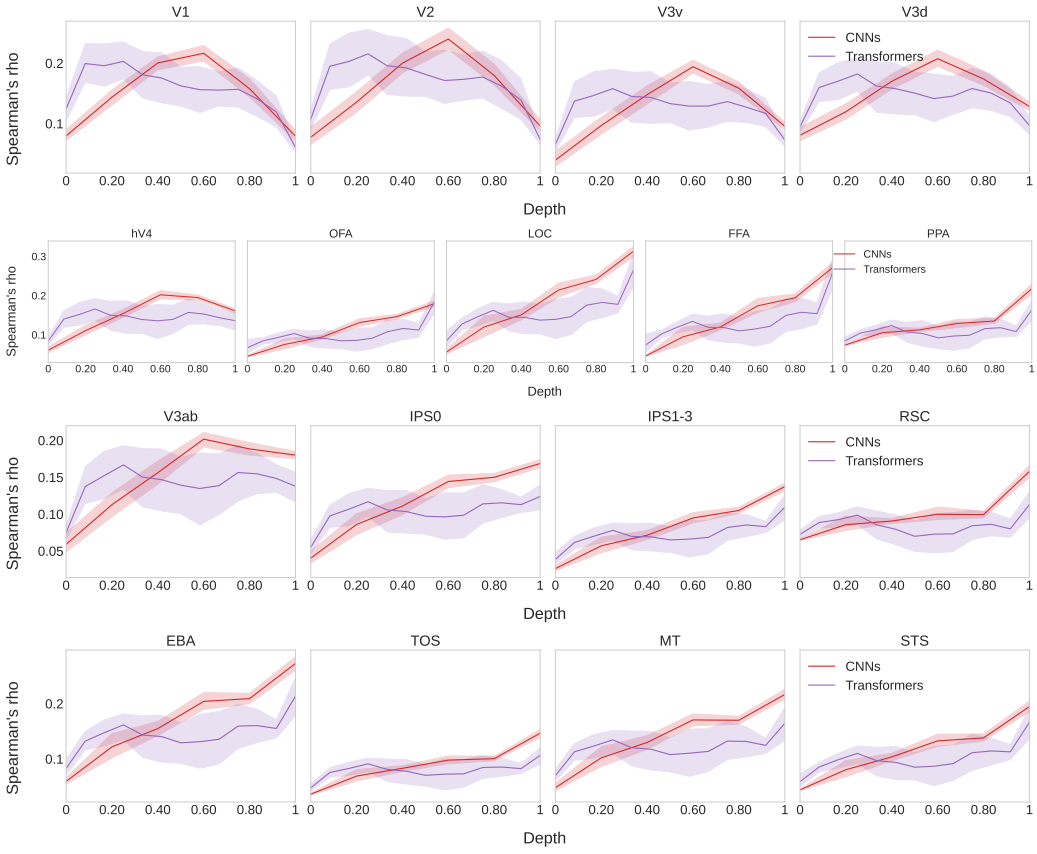

Figure 10: Expanding figure 4a to show all ROIs for the comparison of CNNs and Transformers.

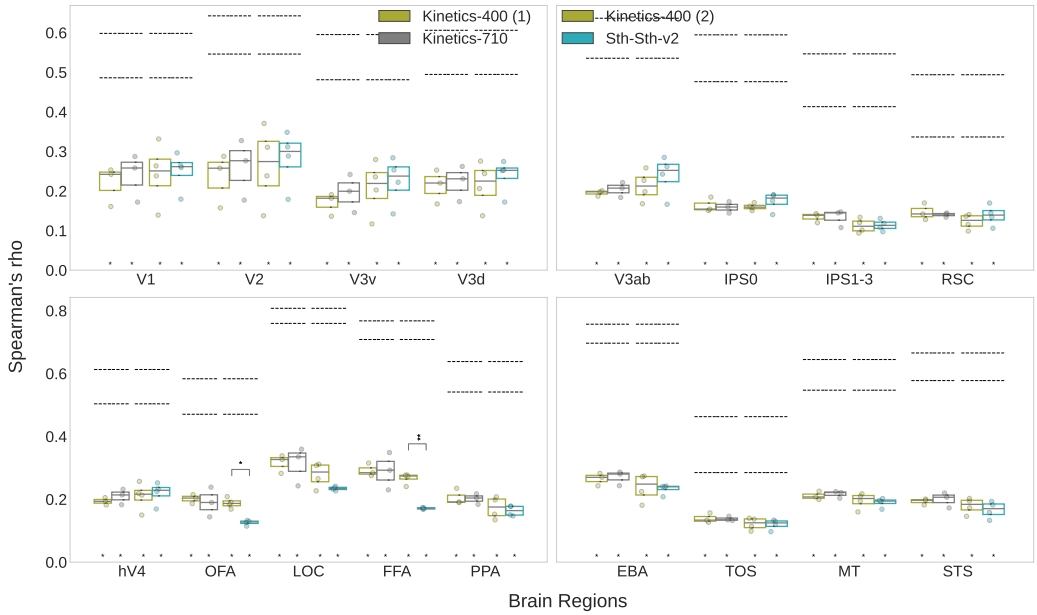

Figure 11: Expanding figure 5a to show all ROIs for the comparison of training datasets.

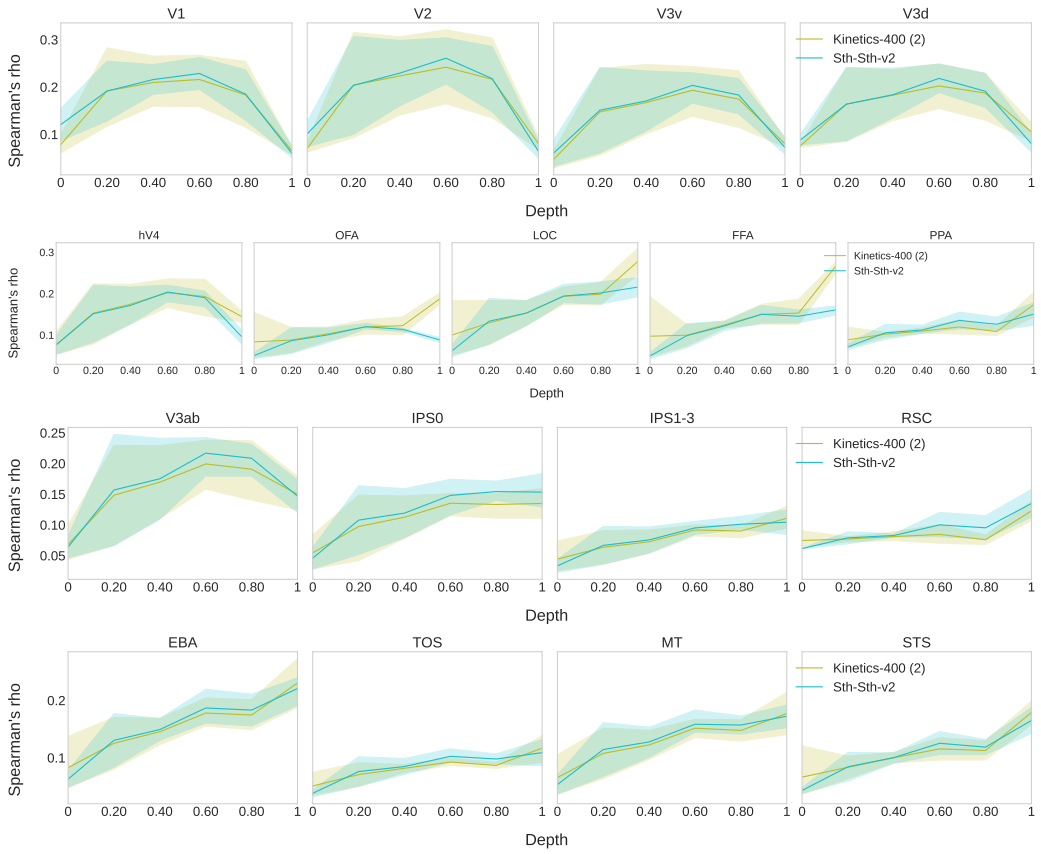

Figure 12: Expanding figure 5b to show all ROIs for the layer-wise comparison of training datasets.

D ADDITIONAL VIEWS

In this section we include alternative ways to produce or view the results of our benchmarking, including different visualization, dimensionality reduction, or set of models.

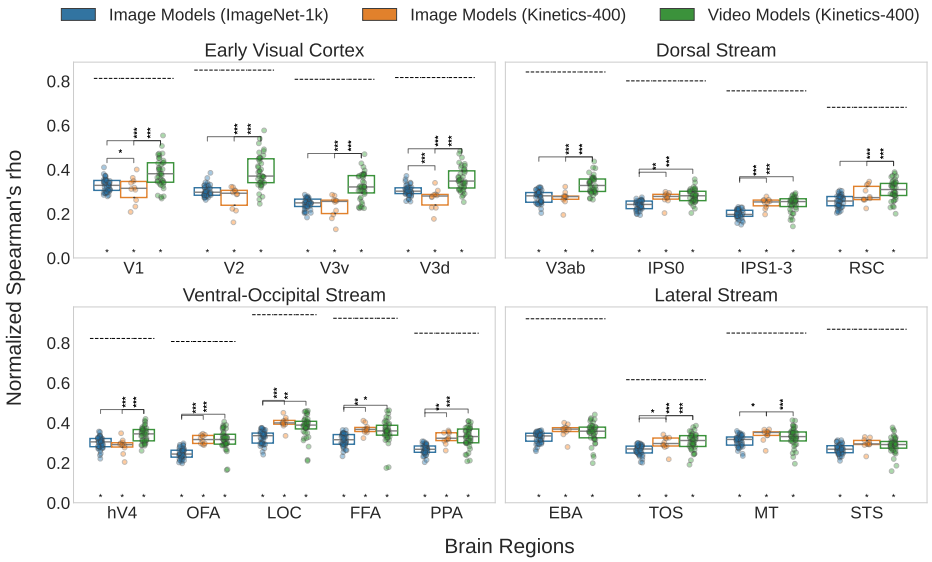

Figure 13: Version of figure 2a, re-scaled to the Upper Noise Ceiling. With this visualization the amount of variance explained is more evident, but the information of ROI noise and absolute correlation is lost.

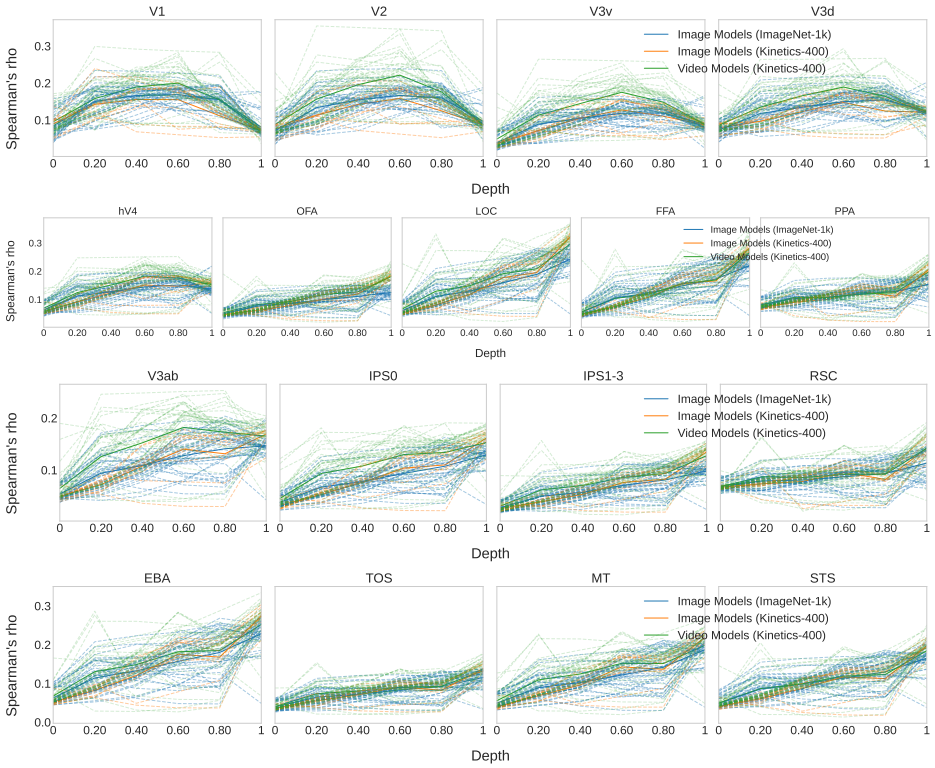

Figure 14: Version of figure 7 with all individual models displayed as separate lines.

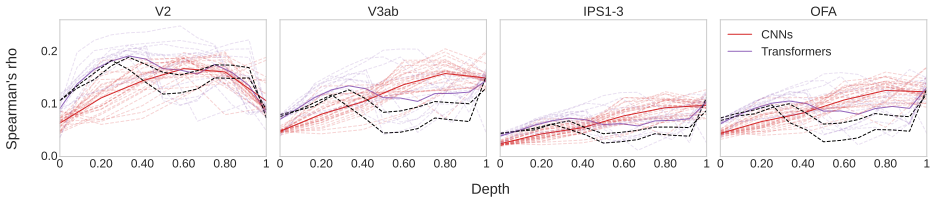

(a)

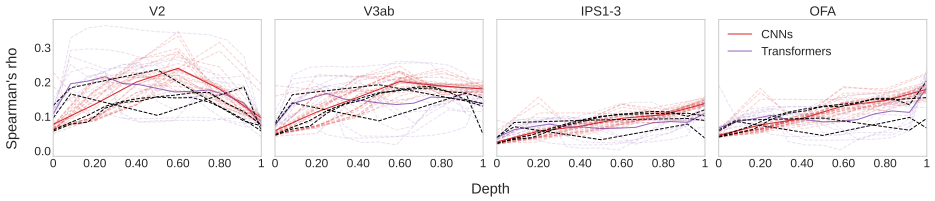

(b)

Figure 15: Comparing hybrid Transformers that include convolution. (a) shows image object recognition models, and black marks ConViT (d'Ascoli et al., 2021). (b) shows video action recognition models, and black marks Uniformer (Li et al., 2023b). ConViT's alignment is similar to the other image Transformers, while Uniformer seems to fall in between video CNNs and Transformers.

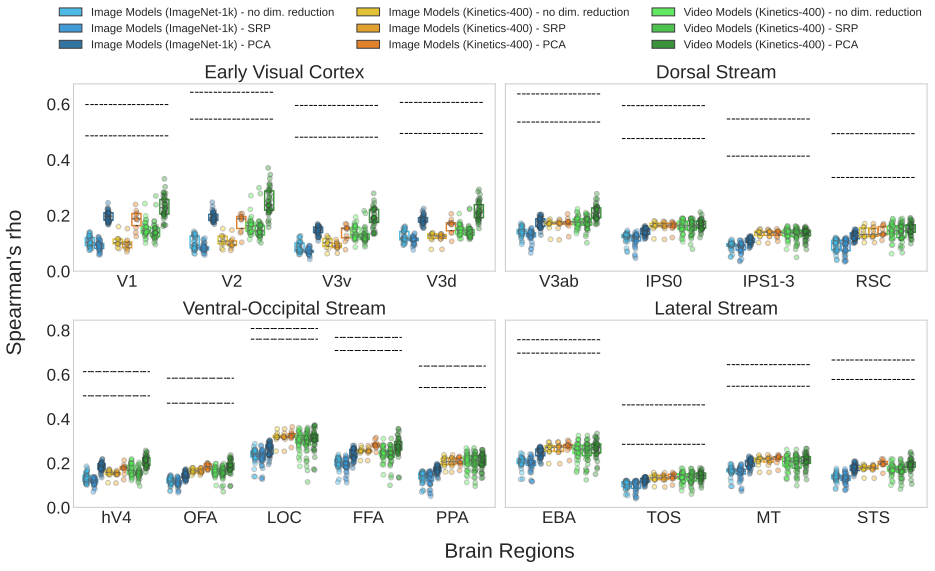

(a)

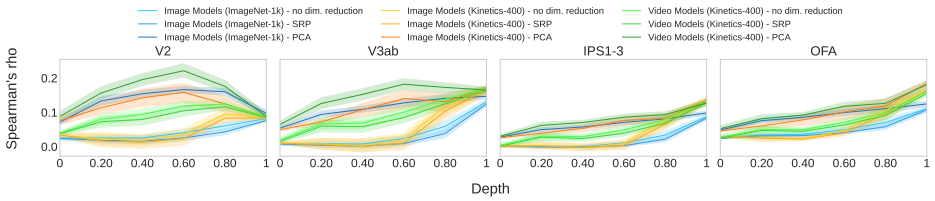

(b)

Figure 16: Dimensionality reduction method comparison on the analysis from figure 2; using Principal Component Analysis (PCA) vs. using Sparse Random Projection (SRP) vs. no dimensionality reduction. Overall, models' RDMs match the brain less when constructed with full dimensions than when keeping important components - same with SRP where the dimensionality is still high.

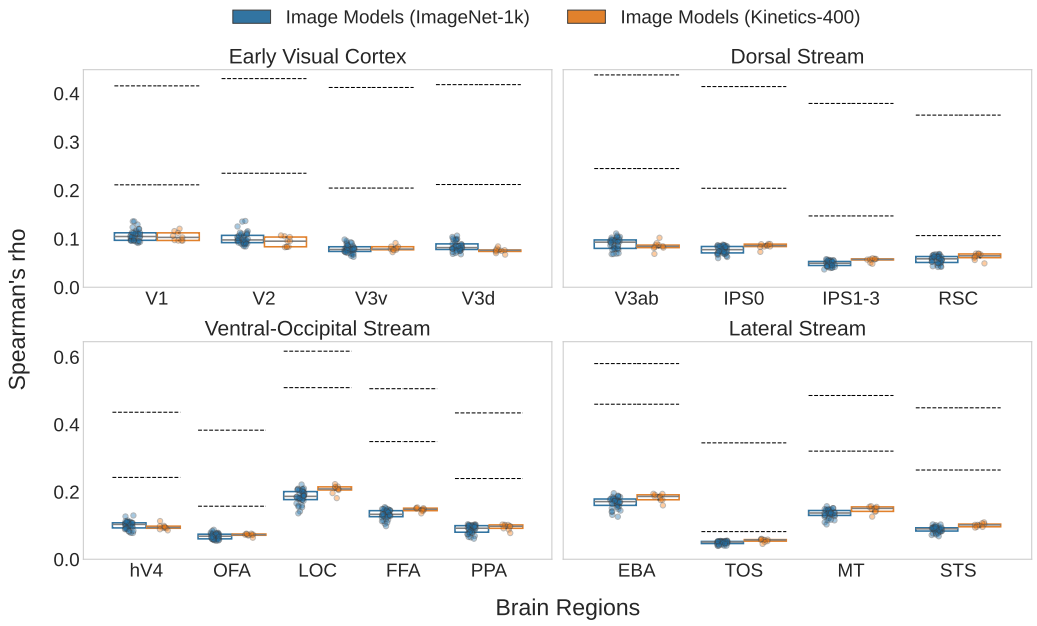

(a)

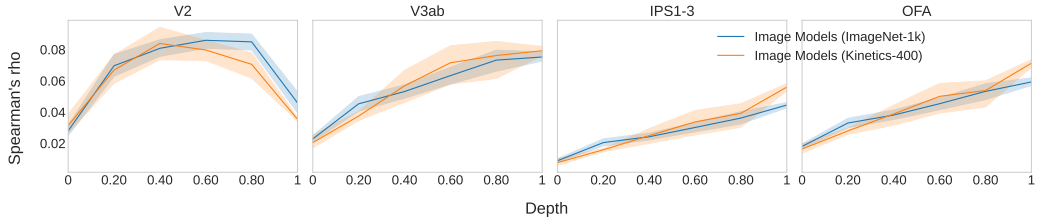

(b)

Figure 17: Image model results (analysis from figure 2) with the 3-repetition 1000-video training set instead of the 10-repetition 102-video test set. Both noise ceilings and model scores drop significantly from figure 2 due to increased measurement noise from the fewer stimulus repetitions.

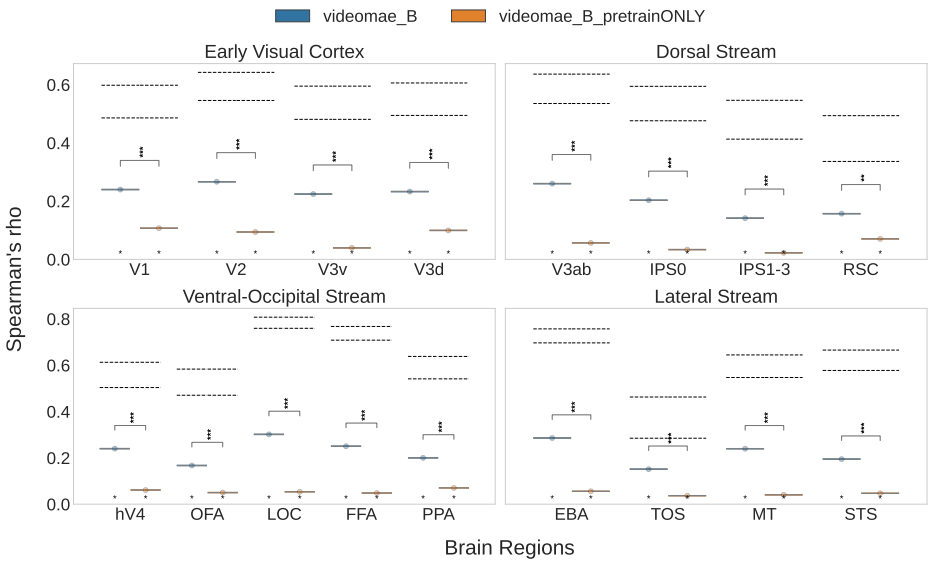

Figure 18: Comparison of the self-supervised model videomae_B, with and without (videomae_B_pretrainONLY) supervised finetuning on Kinetics 400.

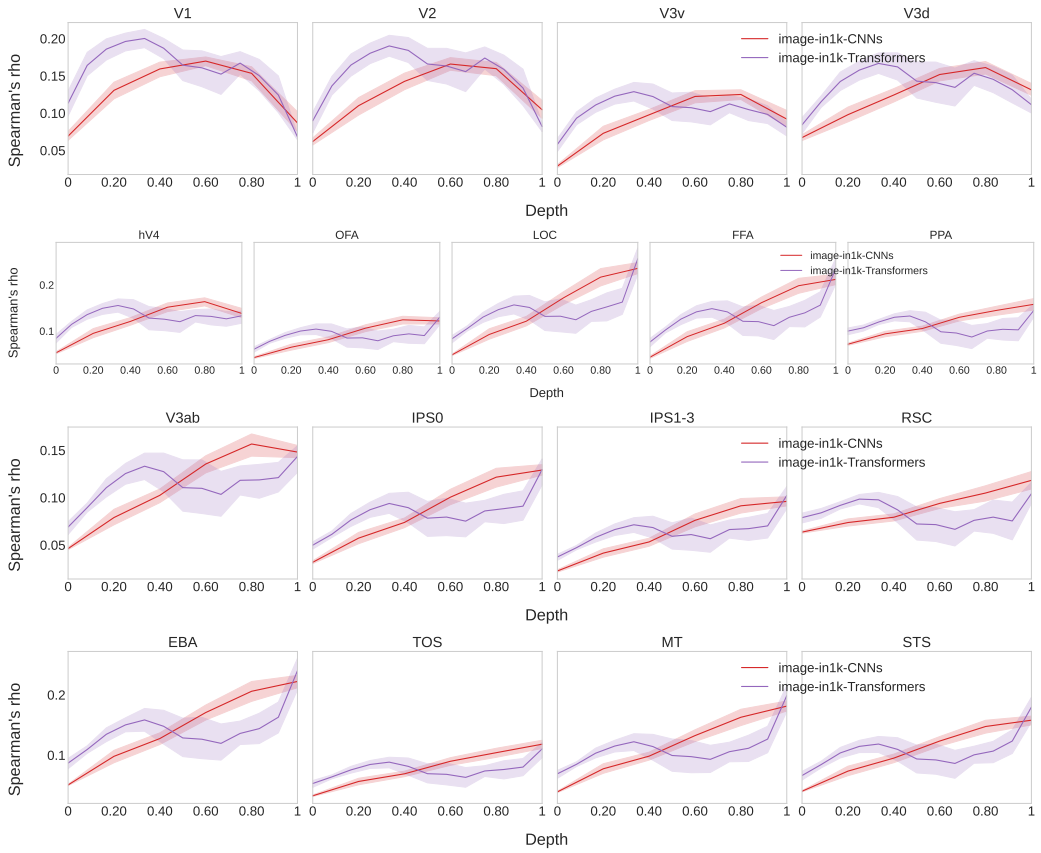

Figure 19: Layer hierarchy for image object recognition CNNs and transformers, plotted as in figure 4b.

E RELATION TO PARAMETERS & ACCURACY

In this section we provide results for the relation of the RSA score to model parameters and model accuracy.

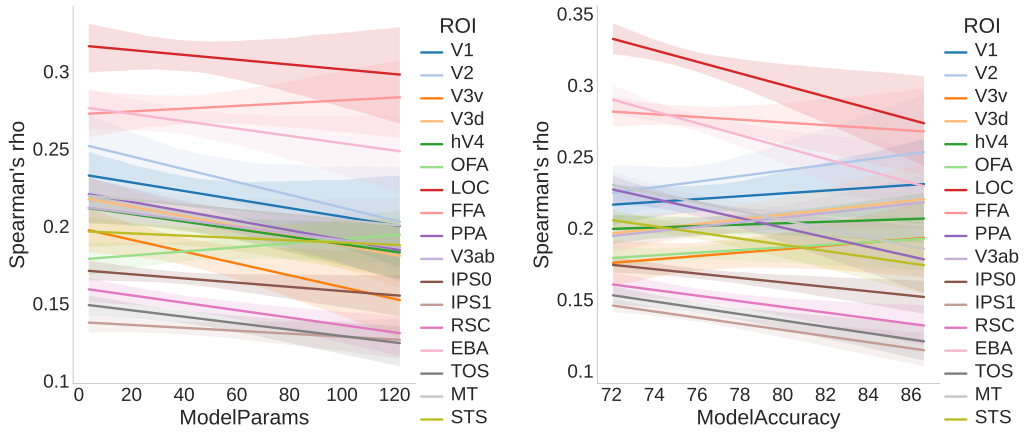

Figure 20: Similar to figure 6a but with model parameters and model accuracy. Here the trends are less consistent than with the model FLOPs.